

Note

Magnetic and optical properties of
trans-*RSSR*-[CrCl₂(cyclam)]₂ZnCl₄
(cyclam = 1,4,8,11-tetraazacyclotetradecane) attributed to
counterion via hydrogen bonding

Marcos Flores-Alamo ^a, Martha E. Sosa-Torres ^{a,*}, Alejandro Solano-Peralta ^a,
Roberto Escudero ^b, Rubén A. Toscano ^c, Miguel Castro ^a, Enrique Camarillo ^d,
José M. Hernández ^d, Héctor Murrieta ^d

^a División de Estudios de Posgrado, Facultad de Química, Universidad Nacional Autónoma de México, Ciudad Universitaria, México, D.F. 04510, México

^b Instituto de Investigaciones en Materiales, Universidad Nacional Autónoma de México, Ciudad Universitaria, México, D.F. 04510, México

^c Instituto de Química, Universidad Nacional Autónoma de México, Ciudad Universitaria, México, D.F. 04510, México

^d Instituto de Física, Universidad Nacional Autónoma de México, Ciudad Universitaria, México, D.F. 04510, México

Received 25 February 2004; accepted 26 June 2004

Available online 12 August 2004

Abstract

This is the first reported example of a photochromic property presented by the change of a counterion in a coordination compound: the colour of the *trans*-[CrCl₂(cyclam)]₂ZnCl₄ (**1**) is dark green while the *trans*-[CrCl₂(cyclam)]Cl (**2**) is reddish purple. The dark green colour of **1** under a fluorescent lamp changes to a deep purple when it is irradiated with an incandescent lamp; when the latter light is turned off, the dark green colour reappears instantaneously, this being a reversible process. Besides, the electron paramagnetic resonance (EPR) spectra of these polycrystalline samples show a very broad isotropic peak centred at $g = 1.995$ for **1** and for **2** a rhombic one at $g = 4.309, 3.107$ and 1.223 . Their molar magnetic susceptibilities, χ_{Mdc} , against temperature (2–300 K) follow Curie Weiss behaviour. For **1**, a low antiferromagnetic coupling ($\theta = -2.78$ K) in the solid state was found as it approaches 2 K, while for **2**, there was found a smaller antiferromagnetic coupling ($\theta = -0.40$ K). From the luminescence studies at 17 K, the lifetime for **1** was found to be twice that for **2**. The crystal and molecular structure of **2** were determined and discussed. Compounds **1** and **2** show the same *trans*-*RSSR* configuration with different hydrogen bonding networks. In **1** the supramolecular array includes intermolecular interactions in which the chromium atoms interact through the zinc atom of the tetrachlorozincate counterion via hydrogen bonding with the extraordinary consequence of showing the previously described physical properties. This has been supported by theoretical calculations, in which it is clearly observed that the HOMO orbital of **1** is a highly delocalised molecular orbital among Cr(III)···Zn(II)···Cr(III), thus giving even more evidence for the strong Cr(III)–Cr(III) interaction through the ZnCl₄ moiety via hydrogen bonding.

© 2004 Elsevier B.V. All rights reserved.

Keywords: Chromium(III); Macrocycles; Zn(II); Supramolecular array; Hydrogen bonding; Luminescence; Energy transfer; Magnetic properties; Density functional theoretical calculations

* Corresponding author. Tel.: +52-55-5622-3808; fax: +52-55-5616-2010.

E-mail address: mest@servidor.unam.mx (M.E. Sosa-Torres).

1. Introduction

New photoactive compounds with special optical and magnetic properties [1] are becoming very important since they might have electronic, electrochemical, photochemical and/or photophysical properties that could serve as a guide in the design of molecular devices. Apart from the interest in the structural and stereochemical aspects [2] as well as the kinetics [3] of octahedral chromium complexes, there has been a growing interest in their photochemical and photophysical properties [4–6]. A counterion effect on the change of colour of the $[\text{Cr}(\text{NO})(\text{NH}_3)_5]^{2+}$ cation has recently been reported. Differences found in the Cr–N–O distances were attributed to the change of the hydrogen bonding strength between the cation and anion, giving rise to different colours of the compounds [7].

The crystal and molecular structure of the dark green *trans*-RSSR- $[\text{CrCl}_2(\text{cyclam})]_2\text{ZnCl}_4$ (**1**) and the deep purple *trans*-RSSR- $[\text{CrCl}_2(\text{cyclam})]\text{NO}_3$ (**3**) complexes [8] have previously been reported. Despite the similarities between their molecular and crystal structures, they differ dramatically in their optical properties. The *trans*- $[\text{CrCl}_2(\text{cyclam})]\text{Cl}$ (**2**) behaves very similarly to **3**.

In order to understand the origin of these differences a structural, magnetic and optical study on complexes **1** and **2** was carried out. Thus, this paper describes the molecular structure, hydrogen bonding interactions, electron paramagnetic spectroscopy and molar magnetic susceptibility as a function of temperature, absorption and emission spectra and lifetimes in the solid state for compounds **1** and **2**. The molecular structure of compound **2** is thus described for the first time. Besides a theoretical density functional calculation of all-electron type at the local spin density level was performed for compounds **1** and **3**, the results being discussed in terms of the observed phenomenon.

2. Experimental

2.1. Syntheses

trans-RSSR- $[\text{CrCl}_2(\text{cyclam})]_2\text{ZnCl}_4$ (**1**) was prepared as published [8]. *trans*- $[\text{CrCl}_2(\text{cyclam})]\text{Cl}$ (**2**) was prepared by a slight modification of the reported technique [3c]. *Anal.* Calc. for $\text{C}_{20}\text{H}_{48}\text{Cl}_8\text{Cr}_2\text{N}_8\text{Zn}$ (**1**): C, 28.14; H, 5.67; N, 13.30; Cl, 33.22. Found: C, 28.30; H, 5.54; N, 13.17; Cl, 33.81%. *Anal.* Calc. for $\text{C}_{10}\text{H}_{24}\text{Cl}_3\text{CrN}_4$ (**2**): C, 33.49; H, 6.74; N, 15.62; Cl, 29.61. Found: C, 33.73; H, 6.89; N, 15.54; Cl, 29.57%.

2.2. Single-crystal X-ray diffraction

A single crystal of **2** was attached to a thin glass fibre using epoxy resin. The data collection and structure

refinement followed a routine procedure. The structure was solved using SIR-97 [9] and refined using SHELXL-97 [10]. Summary of crystallographic data and experimental conditions are listed in Table 1.

2.3. Magnetic susceptibility measurements

These measurements were obtained by using a Magnetic Faraday Balance at 300 K. Diamagnetic corrections were made by using Pascal's constants and the set-up was calibrated with $\text{Hg}[\text{Co}(\text{SCN})_4]$ as standard. A SQUID MPMS-5 Quantum Design Magnetometer was used for measuring the magnetic susceptibility as a function of temperature (2–300 K).

2.4. EPR measurements

These measurements were carried out on polycrystalline samples at X-band on a Jeol JES-TE 300 spectrometer operating at a 100 kHz modulation of the magnetic field and equipped with an X-band low temperature accessory for the experiment at 140 K. The *g* value was calculated from the accurate measurements of magnetic field and frequency parameters.

2.5. Electronic spectra

The absorption and emission spectra and lifetimes were taken using single crystals of the same crop used for the X-ray structural analysis. The sample was prepared in a form of a pellet with KBr. The diffuse

Table 1
Crystallographic data for **2**

Formula	$\text{C}_{10}\text{H}_{24}\text{Cl}_3\text{CrN}_4$
Formula weight	358.68
Colour/habit	red-purple/hexagonal prism
Crystal size (mm)	$0.60 \times 0.32 \times 0.24$
Crystal system	tetragonal
Space group	$P4_2/m$
<i>Z</i>	2
<i>T</i> (K)	293(2)
<i>a</i> (Å)	7.6245(7)
<i>b</i> (Å)	7.6245(7)
<i>c</i> (Å)	13.623(1)
β (°)	90.00
<i>V</i> (Å ³)	791.95(12)
<i>F</i> (000)	374
<i>D</i> _{calc} (g/cm ³)	1.504
Radiation	Mo K α
λ (Å)	0.71073
μ (mm ⁻¹)	1.218
Absorption factor min/max	0.637/0.747
Standard variation (%)	2.8
($\sin \theta/\lambda$) _{max} (Å ⁻¹)	0.7035
Final <i>R</i> on <i>F</i>	0.0311
Final <i>wR</i> on <i>F</i> ²	0.0701
Data/parameters	1199/72
Residuals min/max (e Å ⁻³)	−0.25/0.32

reflectance spectrum was recorded with a Cary 5E UV/Vis/NIR spectrophotometer. For the emission spectra the sample was mounted on a copper sample holder of an Air Products helium closed cycle cryostat. The excitation wavelength was 532 nm of the Spectra Physics-CGR150 YAG-Nd. Lifetime data were obtained from the exponential decay curve and the resultant signals were averaged and saved in an Infinium 500 MHz Hewlett-Packard Digital Oscilloscope.

2.6. Theoretical *ab initio* calculations

A theoretical study was performed by using the code deMon-KS [11], which is a DFT-LCGTO-based method. Calculations were of the all-electron type at the local spin density level of theory [12], orbital basis sets of DZVP2 quality being used. In addition, the Unichem Package was used for the visualisation of the geometries and molecular orbitals.

3. Results and discussion

The colour of **1** is dark green while **2** is a reddish purple. The dark green colour of **1** under a fluorescent lamp changes to a deep purple when it is irradiated with an incandescent lamp; when the latter light is turned off, the dark green colour reappears instantaneously, this being a reversible process (Fig. 1). In order to understand how the counterion in **1** interacts in this compound, several studies in the solid state were carried out.

The crystal and molecular structure analysis of **1** and **2** shows that both have the same *trans*-RSSR configuration with very similar bond lengths and angles. Cr–N(4) 2.058(3), Cr–N(1) 2.074(3) Å and CrCl(1) 2.3472(9) Å for **1**, while for **2** Cr–N(1) 2.0605(16) Å and Cr–Cl(1) 2.3295(6) Å. Angles N(4)–Cr–N(1) 86.0(1)° and N(4A)–Cr–N(1A) 94.0(1)° for **1** and N(4)–Cr–N(1) 85.14(10)° and N(4A)–Cr–N(1A) 94.86(10)° for **2**. Hydrogen bonding between amine protons and chlorine atoms in the corresponding counterions are: H(4)···Cl(1) 2.54(4) and H(1)···Cl(1) 2.73(4) Å for **1** and H(1)···Cl(1) 2.70(3) Å for **2**, although these are also similar (Fig. 2), in their tetragonal crystal system, they show different hydrogen bonding networks.

In the crystal lattice four symmetry related *trans*-[CrCl₂(cyclam)]⁺ cations are hydrogen bonded in a tet-

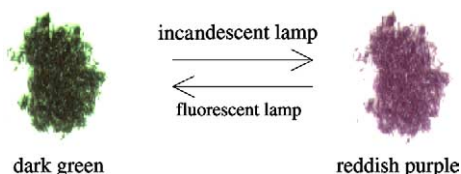


Fig. 1. Illustration of the reversible change of colour shown by **1**.

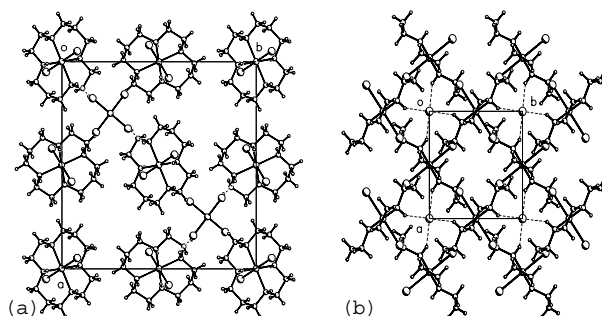


Fig. 2. View looking down the crystallographic *c*-direction (a) for **1** [8] and (b) for **2**.

rahedral fashion to the chloride counterion in **2**. It should be noticed that in the case of **1**, there is a crystallographic array which includes the chromium and zinc from the tetrachlorozincate counterion hydrogen bonded. From the above results it can be shown that **1** and **2** have similar geometry arrays but different hydrogen bonding networks.

Another important difference between **1** and **2** in the solid state is shown by their EPR spectra. A very broad isotropic peak is centred at $g = 1.995$ for **1** while **2** shows a rhombic spectrum: $g = 4.309, 3.107$ and 1.223 . In order to get an insight into this phenomenon, their molar magnetic susceptibilities χ_{Mdc} , were studied as a function of temperature (2–300 K).

The magnetic susceptibility of **1** fits the equation which is valid for two independent total spin functions, S_1 and S_2 [13]; thus, **1** and **2** follow Curie Weiss behaviour (Fig. 3). Effective magnetic moments, μ_{eff} , of 5.51 and 3.86 BM at 300 K in the solid state were found for **1** and **2**, respectively; thus, the high value of μ_{eff} for **1** is explained by the presence of two Cr(III) centres in the molecule. From the inset plot, the magnetic moment of **1**, which decreases as the temperature is lowered, can be observed, indicating a low antiferromagnetic coupling ($\theta = -2.78$ K) as it approaches 2 K, while for **2** a smaller antiferromagnetic coupling ($\theta = -0.40$ K) is observed. Thus, **1** presents stronger intermolecular interactions than **2**, which are explained by their particular networks in their crystal-line arrangement.

The diffuse reflectance spectra of **1** and **2** show two broad bands. The lower energy band for **1** lies at 578 nm, while that for **2** at 567 nm; corresponding to the $^4A_{2g} \rightarrow ^4T_{2g}$ electronic transition. The higher energy band maximum is at 409 and 412 nm, for the $^4A_{2g} \rightarrow ^4T_{1g}$ electronic transition, with shoulders at 380 and 376 nm for **1** and **2**, respectively. The lower energy band of **1** is broader and red shifted compared to that of **2**. Although electronic selection rules forbid the $^4A_{2g} \rightarrow ^2E_g$ transition, a few weak, narrow bands appear at lower energy. The energy of the 2E_g level changes very little with the crystal field strength, but the 4T_g levels do

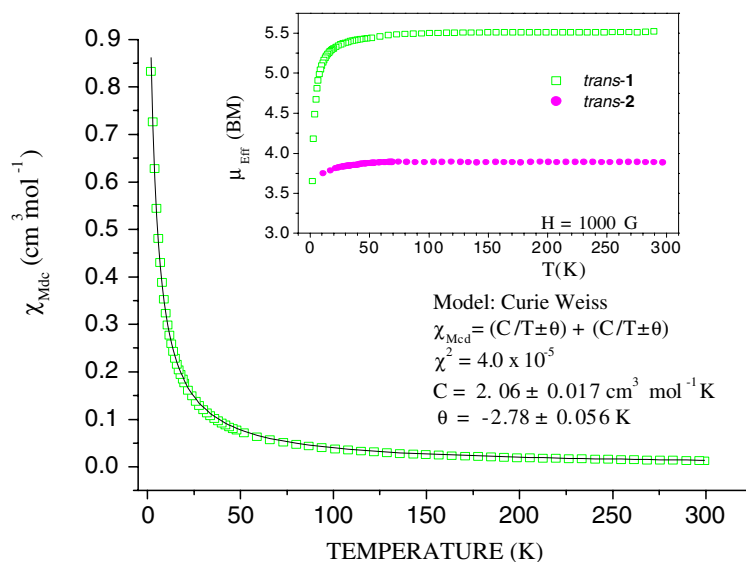


Fig. 3. Plot of χ_{Mdc} vs. T for **1** and μ_{eff} vs. T for **1** and **2**.

change significantly. When white light passes through a sample of **2**, light is absorbed at 567 and 412 nm. The former corresponds to absorption in the yellow-green region of the spectrum and the latter to the violet region (Fig. 4). Because of vibrational interactions, these are broad absorption bands rather than sharp lines which overlap somewhat so that the transmission in the blue is rather small and the absorption curve does not approach the left baseline. In the red region towards 700 nm, absorption falls almost to zero, thus giving **2** its red colour with a slight purple overtone (Fig. 4(b)). For **1**, however, as a result of a lower crystal field, the ${}^4\text{T}_{2\text{g}}$ level is shifted to 578 nm, together with a broadening of this absorption band, and there is an increase in

the yellow-red absorption. The ${}^4\text{T}_{1\text{g}}$ level lies at 409 nm; this absorption band remains in the violet region but, the shape changes slightly, thus, yielding the stronger green transmission and colour for **1** (Fig. 4(c)).

Spin-forbidden transitions for **1** and **2** appear between 660 and 720 nm (inset plot Fig. 4(b) and (c)). Here again the spectrum of **1** shows differences compared with that of compound **2**. At a lower temperature it can be observed that these absorption bands correspond to the same number of emission transitions.

1 and **2** were irradiated at 17 K with excitation wavelengths of 457, 488 and 514.5 nm under the continuous beam of the argon laser. They were also irradiated with 355 and 532 nm of the pulsed beam of the YAG-Nd

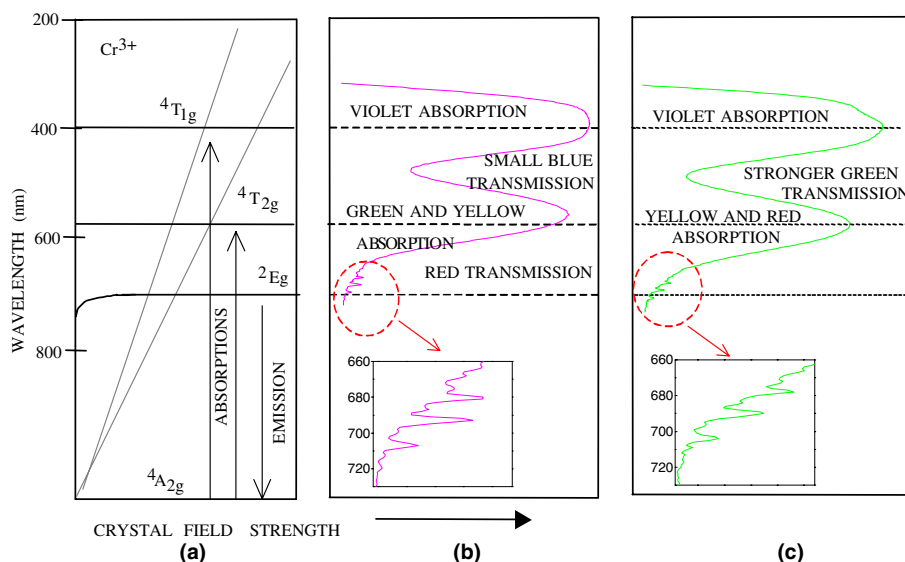


Fig. 4. Term diagram of Cr^{3+} in a distorted octahedral ligand field: (a) diffuse reflectance spectra at 298 K; (b) for **2**, (c) for **1**.

laser. Luminescence of each compound is reproducible under different excitation sources. **1** responds in a different way to the laser excitation of that of **2**, which is consistent with their absorption spectra. The emission spectra (17 K) seem noticeably more sensitive than the absorption. Besides a Stokes shift to lower energy, the spectrum of **1** shows different structure and texture (see Fig. 5).

In addition, compound **1** is shown to have a lifetime value of 60 μ s, compared to that of 30 μ s for **2**. Differences found in lifetime values for double-complex salts have been interpreted due to energy transfer process [14]. Thus, an energy transfer between the chromium(III) atoms of the complex cations through the tetrachlorozincate anion via hydrogen bonding must be taking place and must strongly depend on the mutual relative orientation between the cations and the anion complexes in **1**.

The already described results have been supported by a theoretical calculation [11,12]. The HOMO–LUMO separation reproduces reasonably the 10Dq value found experimentally for compounds **1** and **3**. The HOMO–LUMO separation for **3** is 238 kJ/mol (503 nm), this value is in agreement with the experimental one 211 kJ/mol (567 nm), while for **1**, the HOMO–LUMO separation is 221 kJ/mol (542 nm). This theoretical estimation is close to the experimental one of 207 kJ/mol, (578 nm). The HOMO orbital of **1** is a highly delocalised molecular orbital among Cr(III)–Zn(II)–Cr(III), thus giving evidence for the strong Cr(III)–Cr(III) interaction through the ZnCl₄ moiety via hydrogen bonding (Fig. 6).

This is in contrast with *trans*-RSSR-[CrCl₂(cyclam)]-NO₃, which is analogous to **2**, where the HOMO molecular orbital has a strong d character with significant contributions of the axial Cl atoms through their p orbitals, i.e. here the HOMO orbital is localised along the Cl–Cr–Cl axis.

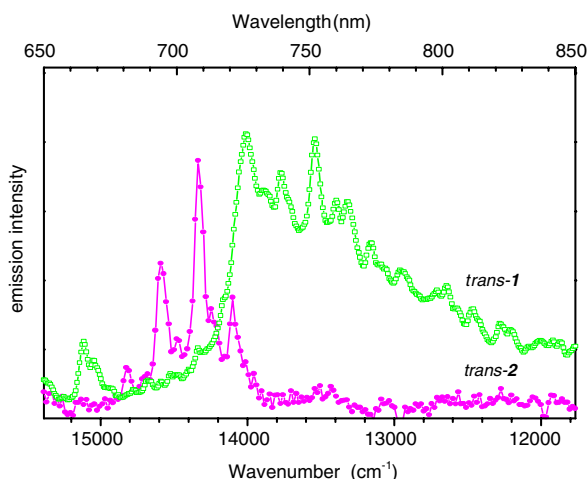


Fig. 5. Emission spectra for **1** and for **2** at 17 K.

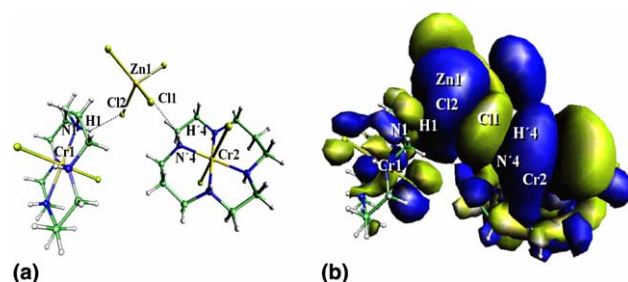


Fig. 6. (a) Intermolecular hydrogen bonding Cr1–N1–H1...Cl2–Zn1–Cl1...H4–N4–Cr2 and (b) HOMO contour plot of complex **1**.

In conclusion, the differences in colour, *g* values in EPR, antiferromagnetism, emission spectra and lifetimes found between **1** and **2** can be attributed to the differences in their hydrogen bonding networks. Thus, in the case of **1**, the supramolecular array includes intermolecular interactions in which the chromium atoms interact through the zinc atom of the tetrachlorozincate counterion via hydrogen bonding with the extraordinary consequence of showing the previously described physical properties. This has been supported by the theoretical calculation in which it is clearly observed that the HOMO orbital of **1** is a highly delocalised molecular orbital among Cr(III)–Zn(II)–Cr(III), thus giving evidence for the strong Cr(III)–Cr(III) interaction through the ZnCl₄ moiety via hydrogen bonding.

4. Supplementary materials

Crystallographic data for the structures reported in this paper have been deposited with the Cambridge Crystallographic Data Centre.

Acknowledgements

The authors are grateful to DGAPA-UNAM (Research Project IN117200). M.F.A thanks CONACyT and DGEP-UNAM for the Ph.D. Scholarship.

References

- [1] (a) O. Sato, T. Iyoda, A. Fujishima, K. Hashimoto, *Science* 271 (1996) 49;
(b) O. Sato, T. Iyoda, A. Fujishima, K. Hashimoto, *Science* 272 (1996) 704;
(c) M. Verdaguier, *Science* 272 (1996) 698.
- [2] (a) D.A. House, V. McKee, *Inorg. Chem.* 23 (1984) 4237;
(b) E. Forsellini, T. Parassasi, G. Bombieri, M.L. Tobe, M.E. Sosa, *Acta Crystallogr., Sect. C* 42 (1986) 563;
(c) C.G. Dealwis, R.W. Janes, R.A. Palmer, J.N. Lisgarten, D. Maes, C.D. Flint, D.M.M. Gazi, *Acta Crystallogr., Sect. C* 48 (1992) 1754.
- [3] (a) A. Bakac, J.H. Espenson, *J. Phys. Chem.* 97 (1993) 12249;
(b) J. Ferguson, M.L. Tobe, *Inorg. Chim. Acta* 4 (1970) 109;

- (c) M.E. Sosa, M.L. Tobe, *J. Chem. Soc., Dalton Trans.* (1986) 427.
- [4] (a) C. Kütal, A. Adamson, *Inorg. Chem.* 12 (1973) 1990;
(b) P.E. Hoggard, A. Kirk, *Inorg. Chem.* 32 (1993) 4475;
(c) D.A. Freisen, S.H. Lee, J. Lilie, W.L. Waltz, *Inorg. Chem.* 30 (1991) 1975.
- [5] (a) L.S. Forster, O. Monsted, *J. Phys. Chem.* 90 (1986) 513;
(b) L.S. Forster, *Chem. Rev.* 90 (1990) 331.
- [6] (a) C. Chiorboli, C.A. Bignozzi, M.T. Indelli, M.A. Rampi, F. Scandola, *Coord. Chem. Rev.* 111 (1991) 267;
(b) C.A. Bignozzi, O. Bartolini, C. Chiorboli, M.T. Indelli, M.A. Rampi, F. Scandola, *Inorg. Chem.* 31 (1992) 172.
- [7] H Akashi, T. Yamauchi, T. Shibahara, *Inorg. Chim. Acta* 357 (2004) 325.
- [8] M.L. Flores-Vélez, J. Sosa-Rivadeneyra, M.J. Rosales-Hoz, M.E. Sosa-Torres, R.A. Toscano, *J. Chem. Soc., Dalton Trans.* (1991) 3243.
- [9] G. Altomare, C. Cascarano, A. Giacovazzo, M.C. Guagliardi, G. Burla, Polidori, Camalli, *J. Appl. Crystallogr.* 27 (1994) 435.
- [10] G.M. Sheldrick, *SHELXL-97: Program for Refinement of Crystal Structures*, University of Göttingen, Göttingen, Germany, 1997.
- [11] (a) D.R. Salahub et al., in: J. Labanowski, J. Andzelm (Eds.), *Density Functional Methods in Chemistry*, Springer, New York, 1991;
(b) N. Godbout, D.R. Salahub, J. Andzelm, E. Wimmer, *Can. J. Chem.* 70 (1992) 560.
- [12] (a) S.H. Vosko, L. Wilk, M. Nusair, *Can. J. Phys.* 58 (1980) 1200;
(b) D.A. Dixons, G. Fitzgerald, T. Raeuchle, in: J.E. Bowie (Ed.), *Data Visualization in Molecular Science*, Addison-Wesley, Reading, MA, 1995.
- [13] O. Kahn, *Molecular Magnetism*, VCH, New York, 1993.
- [14] T. Otsuka, A. Sekine, N. Fujigasaki, Y. Ohashi, Y. Kaizu, *Inorg. Chem.* 40 (2001) 3406.